NAZARBAYEV UNIVERSITY

School of Engineering and Digital Sciences

Bachelor of Engineering in

Mechanical and Aerospace Engineering

MECHANICAL CHARACTERIZATION OF FDM PRINTED FIBER REINFORCED POLYMER

By

Sabina Amanzholova

Yerassyl Maulet

Aibat Mukametkali

Principal Supervisor: Professor Didier Talamona

Co-Supervisor: Professor Asma Perveen

April 2026

Declaration

We hereby declare that this report entitled “Mechanical characterization of FDM printed fiber reinforced polymer” is the result of our own project work except for quotations and citations that have been duly acknowledged. We also declare that it has not been previously or concurrently submitted for any other degree at Nazarbayev University.

Names: Yerassyl Maulet, Sabina Amanzholova, Aibat Mukametkali

Date: April 30, 2026

Abstract

Additive manufacturing with fused filament fabrication (FFF) is becoming a highly adopted method for production of lightweight polymer components with complex geometries. Regardless of its advantages, the process still involves dimensional deviations that limit the application of the polymers produced by FFF in accuracy-sensitive fields. PETG (Polyethylene terephthalate glycol) can be reinforced with continuous carbon fiber (CCF). The reinforcement further enables the enhancement of stiffness and strength but the influence of CCF on dimensional accuracy and mechanical performance of printed parts were not yet deeply investigated.

The project measures the geometrical accuracy and the mechanical behavior of PETG and continuous carbon fiber reinforced PETG (CCF -PETG) printed using an Anisoprint A4 system. A dimensional analysis on the artifact 80 x 80 x 4 mm was held using ZEISS T-scan. First experiments used a Taguchi based experimental design to determine the influence of printing speed and extrusion temperature on dimensional accuracy. Initial results show that CCF-PETG always depicts a smaller dimensional deviation on all axes compared to PETG. These advancements have been correlated with slower print speeds, the greater rigidity of continuous fibers, and alleviated thermal deformation during co-extrusion.

Tensile testing of continuous carbon fiber-reinforced PETG (CCF-PETG) specimens printed at 0°, 15°, 30°, 45°, and contour-only fiber orientations revealed a strong dependence of mechanical properties on fiber angle, with 0° specimens achieving the highest mean ultimate tensile strength of 269.3 MPa and a Young's modulus of 44.62 GPa. Both UTS and stiffness decreased monotonically with increasing fiber angle. These results confirm that fiber orientation is an important parameter governing the mechanical performance of FFF-printed CCF-PETG, and that contour-only configurations provide substantial strength and stiffness improvements over the unreinforced polymer.

Table of Contents

1. Introduction and Problem Statement

Fused Filament Fabrication (FFF) is one of the most widespread and readily available additive manufacturing (AM) technologies given its low cost and ability to print complex shapes with minimal tooling. This technology is widely used in engineering, prototyping and production sectors, where advances in material development and extrusion-based reinforcement were the key drivers. Despite the advantages of the mentioned technology, FFF still has limitations in specific areas: dimensional accuracy of FFF printed parts and the mechanical characterization as a result of the layer-by-layer deposition process [6], [7], [26]. Thermal shrinkage, warpage, cooling gradients and anisotropic deposition significantly impacted tolerances and its mechanical properties, which makes it essential to study printing accuracy and mechanical reliability of the FFF printed parts more closely.

Among the compatible thermoplastics for the mentioned technology, polyethylene terephthalate glycol (PETG) is the most famous one given its relative dimensional accuracy stability, reduced warpage, strong interlayer adhesion and higher impact resistance compared to PLA or ABS [1],[21],[25]. PETG is widely used in functional components. However, its performance depends on a set of parameters including nozzle temperature, extrusion rate, layer height, and raster orientation. These dependencies influence not only print accuracy but also tensile and flexural behavior, requiring systematic evaluation under controlled printing conditions.

Integration of continuous fiber reinforcement (CCF) into PETG using co-extrusion technology is the new direction. CCF-PETG composites offer better stiffness, significantly increased tensile strength, and improved load-bearing capacity, making them promising for lightweight structural applications [4], [10], [14], [22]. However, the area of integration of CCF might have an influence on the geometrical fidelity of the parts given altered thermal behavior and resistance to deformation during deposition is still not yet explored. Though several studies already focused on the mechanical properties of FFF printed parts, there are still a small number of those which compare PETG and CCF-PETG in terms of their dimensional accuracy and mechanical behavior.

For this reason, the project aims to address gaps in the literature and assess the impact of continuous carbon fiber reinforcement on dimensional accuracy and mechanical properties of FDM printed PETG parts. This capstone project focuses on the analysis of

dimensional deviations of printed artifacts with standard geometric features and mechanical properties through tensile testing. By analyzing how fiber reinforcement affects accuracy and structural behavior, the study contributes to establishing design guidelines and material selection strategies for FFF components intended for functional and load-bearing applications.

2. Contributions

Sabina Amanzholova has contributed to a comprehensive literature review of the project and formulated the theoretical background for the study. Also, she performed mechanical testing on neat PETG, 0 degree CCG-PETG, 15 degree CCG-PETG, 30 degree CCG-PETG, 45 degree CCG-PETG, contour only CCF-PETG sample specimens.

Yerassyl Maulet has contributed to a design and manufacturing of artifacts for dimensional analysis. Five different versions of the artifact were developed using an iterative approach. With each new version, the scannability of artifacts were improved and the concentration of CCF was increased. Then, five artifacts for each category (PETG, CCF-PETG, and CCF Contour) were manufactured with Anisoprint Composer A4 FDM Printer.

Aibat Mukametkali has contributed to a data gathering and analysis for dimensional accuracy comparison of PETG, CCF PETG and CCF Contour specimens. Fifteen specimens were scanned and measured. The data analysis was performed using Excel and Matlab software.

3. Literature Review

This Section of the report will discuss the findings about the subject from academic publications.

3.1 Dimensional accuracy in FFF manufacturing

Dimensional accuracy is one of the main obstacles while extrusion-based manufacturing processes. There are different reasons behind the deviations between nominal and factual measured values such as shrinkage, warpage, nonuniform cooling and so on. Chaidas et al. discovered the strong relationship between the printing temperature of the PLA artifacts as well as build plate temperature and other ambient conditions can significantly influence the dimensional accuracy of the model [9]. Akbas et al. explored PLA, ABS, and PETG under various process parameter combinations and found that though PETG is better in resisting dimensional changes than ABS. However, it is still quite sensitive to extruder temperature and print speed [1]. It is clear from this that even materials with low shrinkage, like PETG, must have optimized parameters to achieve predictable tolerances.

A number of works have focused on parameters that have an impact specifically on the accuracy of PETG. Raj et al. developed a machine learning-based approach to predict dimensional deviations in parts made from PETG and underlined that layer height, extrusion temperature, and infill orientation all combine to produce nonlinear trends in accuracy [21]. Valvez et al. further identified the same kind of interaction, demonstrating that layer thickness and raster angle interact in their impacts on final part geometry and mechanical strength [25]. Other optimization studies, such as ANOVA-based parameter modeling by O'Drisscoll et al., further reinforce the conclusion that PETG dimensional accuracy cannot be divorced from broader thermo-mechanical behavior in deposition [18].

Even though many papers discuss dimensional accuracy of only-polymer prints, very few of them focus on the CCF composites. Continuous carbon fiber addition causes increased stiffness at deposition that can worsen geometric accuracy, but it also creates internal stresses as the base material and fibers have unmatched coefficients of thermal expansion. Most literature for CCF-PETG focuses on its mechanical performance; thus, there is a large literature gap in determining how fiber reinforcement affects the geometric fidelity of printed artifacts.

3.2 Mechanical Properties of PETG and Fiber-Reinforced Composites

The mechanical behavior of FFF-printed structures is dependent on parameters such as raster angle, infill density, extrusion temperature, and interlayer bonding quality. Several characterizations of these dependencies have been made in the literature for polymer-only materials. Bex et al. and Cuan-Urquizo et al. illustrate that infill orientation, printing direction, and sample geometry significantly affect tensile and flexural properties of FFF structures [4], [6]. Similarly, Mahesh et al. report that layer height and shell thickness are the dominant factors in determining flexural strength [16]. In case of PETG, for instance, Valvez et al. point out the strong correlation between mechanical behavior and layer deposition patterns [25], while Iacob et al. extend the investigation to compare neat PETG with recycled PETG under bending tests [11].

Continuous carbon fiber-reinforced PETG reinforces the way to overcome the mechanical limitations of polymer-only FFF components. Fallah et al. presented the nonlinear mechanical behavior of CCF-PETG composites and addressed the importance of fiber-matrix adhesion and the orientation of fibers with respect to load transfer [10]. Kasmi et al. researched strategies for printing techniques of continuous fiber deposition and have identified fiber path optimization as a key factor to improving strength and stiffness [14]. Lupone et al. and Rijckaert et al. further developed these results by investigating the effects of fiber orientation and strategies for loading fibers, respectively, and show that continuous fibers significantly reinforce mechanical performance if aligned properly [15], [22]. In addition, extended reviews from Jamal et al. summarize the various strategies for reinforcement and conclude that the integration of carbon fiber reinforces the matrix with higher strength-to-weight ratios and improved mechanical stability [12]. Finally, Dairabayeva et al. complement this work by discussing the mechanical analysis with economic considerations and emphasize that CCF-PETG has industrial feasibility and applicability [8].

3.3 Project Focus

While there is significant literature on FFF polymers and their fiber-reinforced composites, most studies have focused solely on either dimensional accuracy or mechanical performance. Indeed, very few works have reported integrated assessments of both aspects using standardized PETG and CCF-PETG specimens fabricated under identical printing conditions. In addition, there is a serious lack of understanding regarding how continuous fiber reinforcement affects geometric deviations and its tensile

behaviour. It is this gap that has motivated the present study, which intends to provide a full comparison of accuracy and mechanical performance between PETG and CCF-PETG materials.

4. Methodology

This section of the capstone report discusses the design of experiment, used materials, equipment and software.

4.1 Design of Experiment

The process of assessing dimensional accuracy of FDM printed parts, it was decided to follow the following procedures:

- Design a geometric artifact for GD&T analysis
- Manufacture artifacts using a suitable FDM printer
- Scan manufactured artifacts using 3D scanner
- Extract data from the scan results
- Analyze collected data

In order to assess the mechanical properties of FDM printed parts the following experimental steps were followed:

- Design tensile specimens
- Manufacture specimens using an FDM printer
- Conduct mechanical testing including tensile tests
- Collect and analyze data

4.2 Materials

This subsection describes and lists the materials used for this capstone project.

4.2.1 Polymer Matrix

Polyethylene Terephthalate Glycol (PETG) thermoplastic filament was used as the polymer matrix for printing. PETG used in this project is a PolyLite™ 1.75 mm Black PETG Manufactured by Polymaker [20].

4.2.2 Composite Reinforcement

Anisoprint CCF 1.5K Composite Carbon Fiber [2] was used as a composite reinforcement material. This reinforcement was pre-impregnated and integrated into

printed specimens using the composite co-extrusion technology by Anisoprint. Reinforcement settings were selected within the slicer software and remained identical to the reinforced specimens of one type.

4.3 Equipment

The following subsection lists and describes the equipment that was used for this capstone project.

4.3.1 FDM Printer

For fabrication of Artifacts and Mechanical testing specimens, it was decided to use Anisoprint Composer A4 FDM Printer [2] the co-extrusion technology provided by this printer allows printing with pre-impregnated continuous carbon fiber composite material. This FDM printer is commercially available and it is present in the materials laboratory.

4.3.2 3D Scanning Equipment

To conduct dimensional analysis, ZEISS T-Scan 3D scanner was used. According to the technical specifications [3], the accuracy of the 3D scanner is 0.033 mm, the measuring depth is 50 mm, and field of view is 2894 mm x 2324 mm. These parameters are suitable for the artifact design, and ZEISS T-Scan 3D scanner allows to digitize the whole surface of the specimen, resulting in more accurate dimensional analysis.

4.3.3 Mechanical Testing Equipment

Tensile specimens are to be printed using Anisoprint Composer A4 FDM printer. Polymer and composite materials are PolyLite™ 1.75 mm Black PETG and Anisoprint 1.5k CCF respectively. CMT-50 Universal Testing Machine [5] is to be used to conduct mechanical testing of manufactured specimens.

4.4 Software

4.4.1 CAD Modeling Software

Specimens design process requires the use of CAD modeling software. SolidWorks 2025 CAD software [24] is used to create CAD models of GD&T artifacts and tensile specimens. Mentioned software is available in the university computer labs and allows to save created CAD models in STL format.

4.4.2 Slicing Software

Created STL files are later uploaded into the pre-processing software in order to set printing parameters and create printing instruction sets for an FDM printer. Since Anisoprint Composer A4 FDM printer is used in this project, it was decided to use Anisoprint Aura pre-processing software [3] to slice the STL files and save instructions in the gcode format.

4.4.3 Metrology Software

Two different types of software were used to conduct GD&T analysis of artifacts. The first software is Zeiss Colin3D. This software is used to collect and post-process data from the 3D scanner [23]. The second software is GOM Inspect. This software is used to measure the dimensions of features and conduct surface comparison analysis [23].

4.5 Artifact Design for GD&T Evaluation

In order to assess the dimensional accuracy of FDM printers it was necessary to design a printable part for further printing and dimensions measuring. 3D printed parts with certain geometrical features are called artifacts. Artifact designs were developed using SolidWorks 2025 CAD software. The table and figure below represent the design evolution of GD&T artifact design.

Figure 1. CAD models of Artifact (Design Evolution)

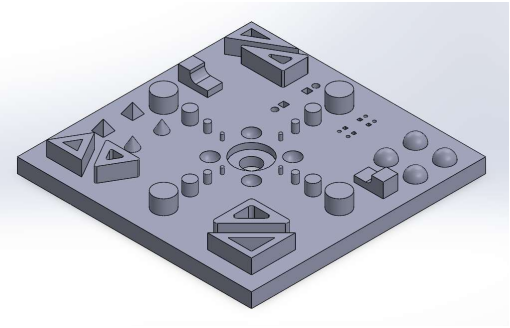

Figure 1 a) Artifact version 1.

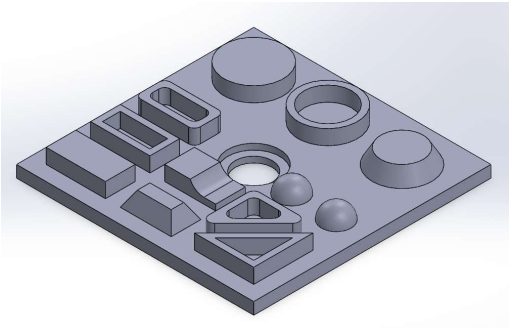

Figure 1 b) Artifact version 2.

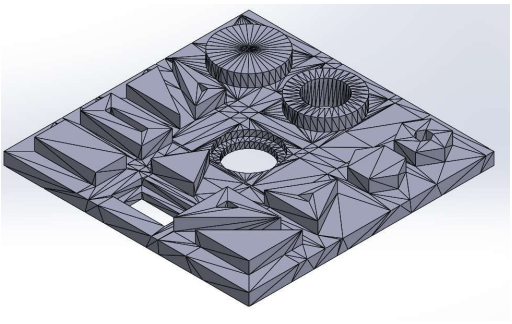

Figure 1 c) Artifact version 3

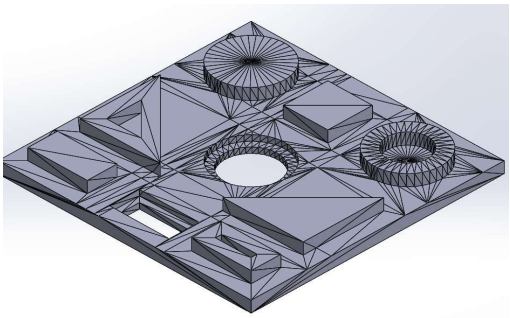

Figure 1 d) Artifact version 4

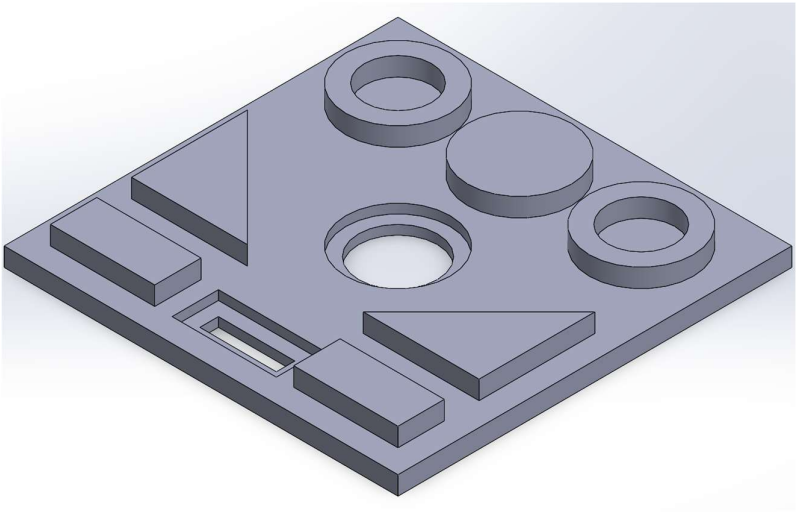

Figure 1 d) Artifact version 5

First version of an artifact had a 80 by 80 mm wide and 5 mm thick base and several geometrical features including cylinders, circular and rectangular holes of different sizes, spherical dents and shapes, triangles of different angular proportions, cones and pyramids. This version of an artifact was necessary to identify the limits of a 3D printer.

Artifact V2 had certain changes compared to version 1. Small features were removed and replaced with bigger shapes as 3D printers could not reinforce small features with continuous carbon fiber. The thickness of the base was reduced to 4mm. Also, rectangular features were added.

Artifact V3 is similar to the version 2, however hemispherical features, cut cones and pyramid features were removed due to measuring difficulties. Rectangular holes were added and features overall were redesigned to be more suitable for CCF-PETG printing.

Artifact V4 is considered as satisfactory in terms of amount of carbon fiber reinforcement, however certain features like hollow triangle feature and extruded square feature created difficulties during the scanning process as the distance between features were not enough for the scanner to scan the surface of an object. Therefore, it was decided to redesign the artifact.

Artifact V5 fixed scan related issues as the hollow triangle feature was replaced by a mirrored version of a regular triangular feature and the extruded square feature was replaced by a cylindrical feature. The current version of the artifact has enough CCF reinforcement and is suitable for scanning using the ZEISS 3D Scanner.

Artifact V5 was accepted as a suitable version in terms of having sufficient amount of CCF reinforcement and being relatively easier to scan. Therefore Figure 2 shows a more detailed drawing of the artifact.

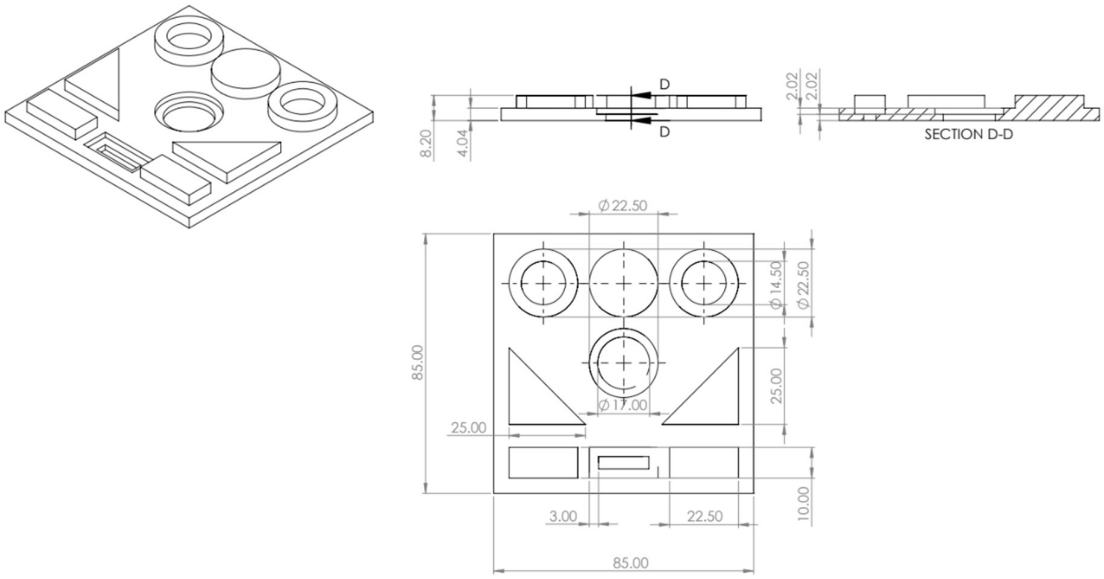

Figure 2. Artifact V5 schematic (dimensions are in mm)

4.5.1 Printing Parameters and Slicing

After designing an artifact CAD model, it is later converted into STL (Standard Triangle Language) format and uploaded into the pre-processing software. Through the trial and error method the optimal printing parameters were identified. Starting from

parameters that are recommended by the filament manufacturer, the following parameters such as printing temperature, buildplate temperature, printing speed, layer height etc were identified. Table 1 represents the optimal printing parameters set for manufacturing the Artifact.

Table 1. Artifact Printing Parameters

Printing Parameter	PETG Artifact	CCF PETG Artifact	Contour Only CCF PETG Artifact
Buildplate Temperature, °C	75	75	75
Polymer Extruder Temperature, °C	230	230	230
Composite Extruder Temperature, °C	-	235	235
Layer h, mm	0.32	0.32	0.32
First Layer h, mm	0.2	0.2	0.2
External Shell Layer h, mm	0.16	0.16	0.16
Printing speed, mm/s	30	30	30
First Layer Printing Speed	30	30	30
Composite Extruder Speed Multiplier	-	0.5	0.5
External Shell Flow Multiplier	0.98	0.98	0.98
Infill Density, %	100	100	100
Infill Pattern	Zigzag	Zigzag	Zigzag
Plastic Infill Orientation	45/-45	45/-45	45/-45
Reinforced Infill Orientation, degrees	-	45/-45	-

4.5.2 Artifact Fabrication

After pre-processing the model and converting into a gcode instructions set format files were later uploaded into an SD card which was inserted into the corresponding port on the FDM printer. The buildplate of the printer is made of glass and an adhesive glue was applied on the surface of a buildplate to ensure proper adhesion of the first layer. Both polymer and composite extruders were cleaned using a brass metal brush and paper towels between each print. Filament material was dried at a temperature of 65 ℃ for 5-6 hours before printing. Overall 10 GD&T Artifacts were manufactured including 5 PETG specimens and 5 CCF-PETG specimens. It is planned to manufacture a batch of 5 specimens where CCF is used only while printing the contour of an artifact. Figure below shows the print results of Artifact V5.

Figure 3. Artifact V5 Print Results

4.5.3 3D Scanning procedure

The 3D Scanning procedure starts with the calibration of the scanner. This is necessary to ensure the accuracy of the scanner. The calibration process is done using a special sphere. The surface of the sphere is scanned, and the scanner compares the data with the default data for the sphere. The calibration was conducted each week. The results of the calibration are shown on the figure below.

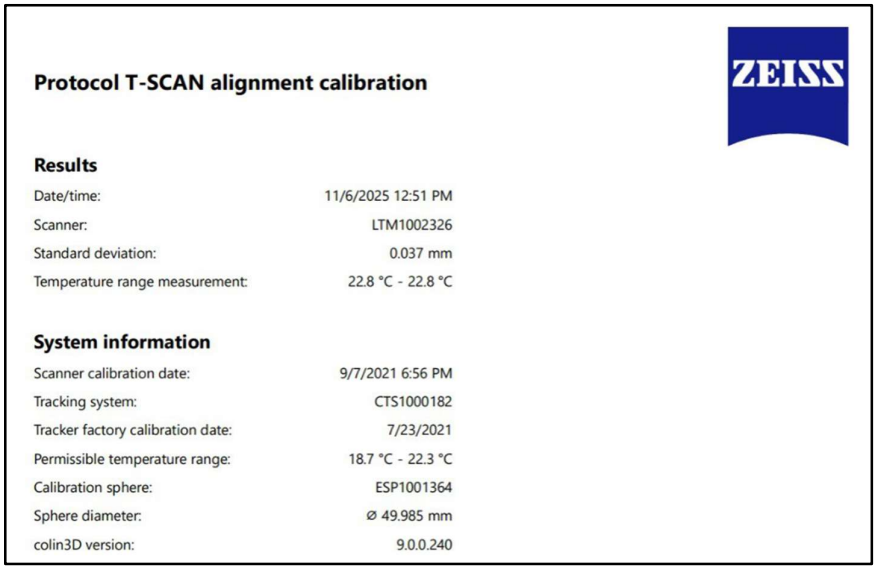

Protocol T-SCAN alignment calibration

ZEISS

Results

Date/time:	11/6/2025 12:51 PM
Scanner:	LTM1002326
Standard deviation:	0.037 mm
Temperature range measurement:	22.8 °C - 22.8 °C

System information

Scanner calibration date:	9/7/2021 6:56 PM
Tracking system:	CTS1000182
Tracker factory calibration date:	7/23/2021
Permissible temperature range:	18.7 °C - 22.3 °C
Calibration sphere:	ESP1001364
Sphere diameter:	⌀ 49.985 mm
colin3D version:	9.0.0.240

Figure 4. ZEISS T-SCAN calibration results

After the calibration is done, the scanning process is started. The data is collected with Zeiss Colin3D software. In this step, it is important to scan the maximum surface area, without letting blind spots. This is achieved by finding the optimal scan parameters that suit the surface of the artifact. The reason is that the surface parameters, like the color of a specimen, affect the quality and time that takes to scan an object. The set of parameters were chosen based on the manual to the 3D scanner. After the scanning process is finished, the raw data has some discrepancies. This can be seen from the figure below.

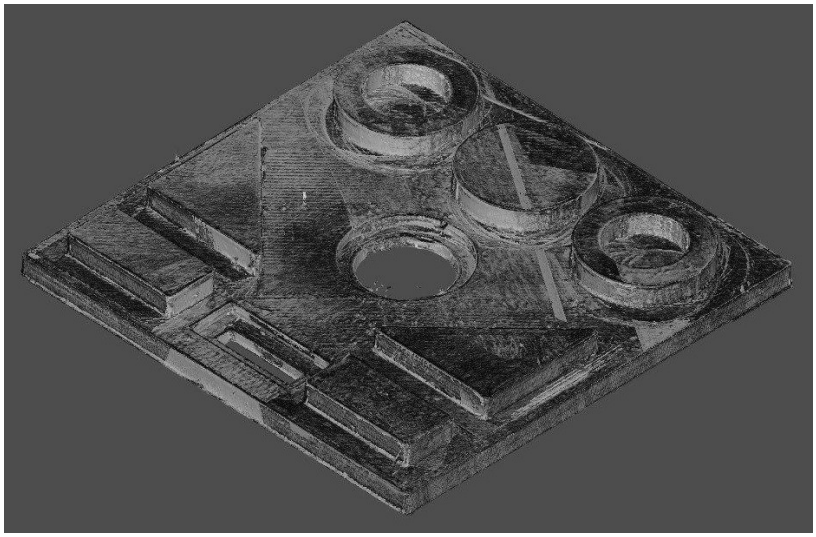

Figure 5. raw data from the scanner

The next step is to optimize the data and remove the discrepancies. This is done by the Colin3D software. After this process, the mesh data is obtained, and it can be seen in figure 6.

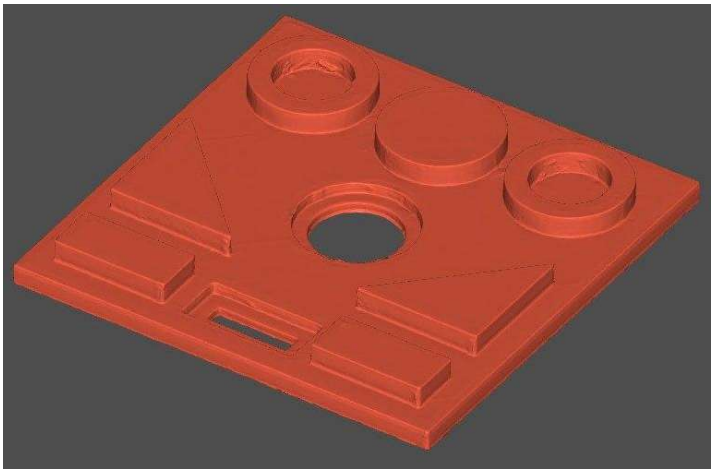

Figure 6. mesh data

4.5.4 Measurement and Surface Deviation Analysis Workflow

Then, the mesh data is imported into the GOM Inspect software. This is the main software which is used to conduct the dimensional analysis. Firstly, the mesh data is aligned with the CAD model. This is done using the Prealignment function of GOM Inspect software. Secondly, the surface comparison is carried out using the corresponding function in GOM Inspect software. This function calculates the distance from each point in the mesh to the corresponding CAD model point. The result of this comparison is the map of deviations, ranging from negative to positive. The negative deviation is shown with blue color, the zero deviation with green, and the positive deviation with red color. All surface comparison data is shown in the appendix, the figure below shows the surface deviation for the PETG specimen:

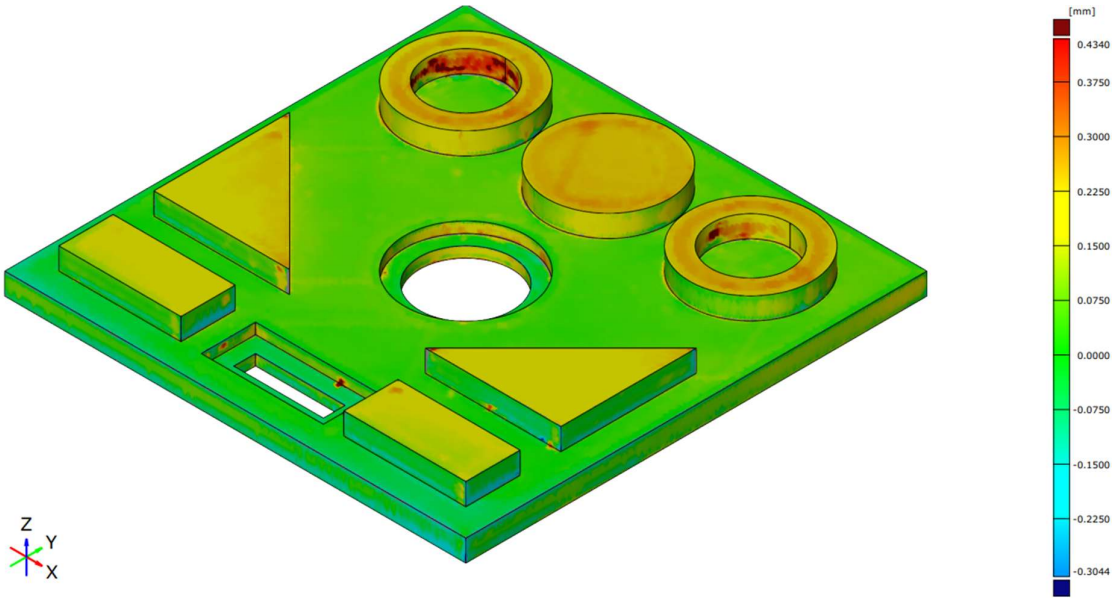

Figure 7. The surface comparison for the PETG sample.

The next step is measuring the dimensions of features. Four different functions were used in the software. These are Auto Cylinder, Auto Plane, Outer Disc Caliper, and Inner Disc Caliper functions. For cylindrical shapes, Auto Cylinder function was used to measure the diameter and height. This function calculates the best-fit cylinder for the given data taking into account all the points from the scanned data. This method ensures that the average diameter is measured for the cylinder. Auto Plane function is used to measure the length of rectangular shapes. This function creates the best-fit planes for rectangular shapes. Then, the distance between the intersection points of planes is measured as a length of a rectangular feature, assuring that the average distance is measured. The next two functions, Outer Disc Caliper and Inner Disc Caliper are used to measure when the Auto Plane function could not be used. These functions measure the distance as calipers, but they are more accurate, because the human error is removed from measurements.

4.5.5 Dimensional accuracy Analysis

Dimensional data were collected from a total of 15 printed specimens. For each specimen, 29 independent dimensions were measured. Consequently, each feature category contains five-dimensional deviation values corresponding to the five specimens. To compare the dimensional accuracy between materials, the mean deviation and standard

deviation were calculated for each category. Prior to computing these statistics, the normality of the data distributions was evaluated.

Normality, the degree of perpendicularity of the features with respect to the surface, was assessed using the Shapiro–Wilk test, which is commonly recommended for small sample sizes ($n < 50$) due to its high statistical power [28]. Since each category in this study contains five measurements, the test was applied individually to each category using MATLAB R2025b. In total, 29 feature categories per material were analyzed. A significance level of $\alpha = 0.05$ was used to evaluate the null hypothesis that the data follow a normal distribution. For the PETG specimens, only one category rejected the null hypothesis, namely the right triangle dimension in the x-direction. This deviation is attributed to one measurement that differs noticeably from the remaining values, which are otherwise closely clustered.

The same procedure was applied to the CCF-PETG specimens. In this case, six out of the 29 categories rejected the null hypothesis. These correspond to the base dimension in the x-direction, middle cylinder in the z-direction, outer diameter of the right cylinder, CCylinder2 d, RTriangle l, and CMRectangle l.

For the Contour-PETG measurements, none of the analyzed categories rejected the null hypothesis. Therefore, the majority of the examined feature categories did not show statistically significant deviations from normality.

For each feature group and material type, the mean value and standard deviation of the dimensional deviations were calculated. The numerical results are summarized in Table 1. Figure 4 (a, b) presents a graphical visualization of the measured data. In addition, box plots were constructed to compare the variability of different feature groups and materials.

4.5.6 Tensile testing procedure

Tensile testing was conducted using a CMT-50 universal testing machine to evaluate the mechanical properties of neat PETG and continuous carbon fiber-reinforced PETG (CCF-PETG) specimens. The specimens tested included neat PETG, as well as CCF-PETG printed at fiber orientations of 0°, 15°, 30°, and 45°, along with a contour-only CCF-PETG configuration. The procedure followed for all specimen groups was as described below.

4.5.7 Equipment Setup and Specimen Preparation

The CMT-50 universal testing machine was powered on and the accompanying testing software was launched. Prior to mounting each specimen, the gauge dimensions at the narrowest cross-section (the neck region, where fracture was expected to initiate) were measured using digital callipers. Specifically, the width and thickness of the neck were recorded and entered into the software to allow accurate stress calculations during the test. The material parameters within the software were configured according to the specimen type being tested, using the standard settings applicable to polymeric materials.

4.5.8 Specimen Mounting and Extensometer Attachment

Each specimen was gripped securely in the machine's upper and lower pneumatic clamps, ensuring correct alignment along the loading axis to minimise bending or eccentricity during the test. A clip-on extensometer was then attached at the center of the gauge length to provide accurate local strain measurements during the elastic and early plastic deformation phases. Before initiating the test, all load, displacement, and strain readings were zeroed to eliminate any pre-load or offset errors.

4.5.9 Test Execution

The test was initiated by pressing the start button in the software, which applied a monotonically increasing tensile load at the prescribed crosshead speed(5mm/min). The test proceeded in two distinct phases:

- During the initial linear (elastic) phase, the extensometer recorded strain data. The software was configured to prompt the operator to remove the extensometer at a defined threshold specifically, at the point where the stress-strain response was about to deviate from linearity to prevent damage to the instrument upon specimen fracture.
- Upon receiving the on-screen removal prompt, the extensometer was carefully detached within a 10-second window, after which the test continued to run until final fracture of the specimen.

An important procedural adjustment was made between specimen groups: the extensometer removal threshold was modified depending on the material under test. For neat PETG specimens, the threshold was set at a relatively lower load, reflecting the earlier onset of yielding and non-linearity typical of an unreinforced thermoplastic. For CCF-PETG specimens, however, the stress-strain curve remained linear over a

considerably larger load range due to the high stiffness imparted by the continuous carbon fibers; consequently, the removal threshold was set at a higher load to ensure that the extensometer remained in place throughout the entire linear elastic regime and was only removed as the response approached its limit.

4.6 Specimen groups tested

The above procedure was applied consistently to all specimen groups. The six configurations tested were:

1. Neat PETG (unreinforced baseline)
2. 0° CCF-PETG (fibers aligned with the loading direction)
3. 15° CCF-PETG (fibers at 15° to the loading direction)
4. 30° CCF-PETG (fibers at 30° to the loading direction)
5. 45° CCF-PETG (fibers at 45° to the loading direction)
6. Contour-only CCF-PETG (carbon fibers deposited only along the specimen perimeter)

For each configuration, three specimens were tested to ensure repeatability, and the resulting load-displacement and stress-strain data were recorded by the software for subsequent analysis.

4.7 Calendar Plan

PROJECT DATA		GANTT CHART																														
Activity	Assigned to	1	2	3	4	5	6	7	8	9	10	11	12	13	14	15	22	23	24	25	26	27	28	29	30	31	32	33	34	35	36	37
Literature review	Sabina A., Yerassyl M., Aibat M.																															
Artifact development	Yerassyl M.																															
Zeiss T scan data collection	Aibat M.																															
Mechanical properties data collection	Sabina A.																															
Printing specimen for testing	Sabina A. Yerassyl M																															
Final report development	Sabina A., Yerassyl M., Aibat M.																															

Figure 8. Calendar Plan

5. Results

This section of the report demonstrates, validates and discusses the results of experiment within the scope of the capstone project. The results obtained were fully transparent to the best of the team's knowledge. All the waste was disposed as per policy

of Nazarbayev University. Mechanical Tests were done in accordance with ASTM standards.

5.1 Dimensional accuracy results

Table 4 and Figures 9 and 10 show that no particular trend in dimensional accuracy can be observed across the materials investigated. For the largest dimensions, b1 and b2, the smallest deviations were obtained with Contour PETG (158 µm and 3 µm, respectively). In the y-direction, PETG exhibited a smaller deviation (163 µm) compared to CCF-PETG (183 µm).

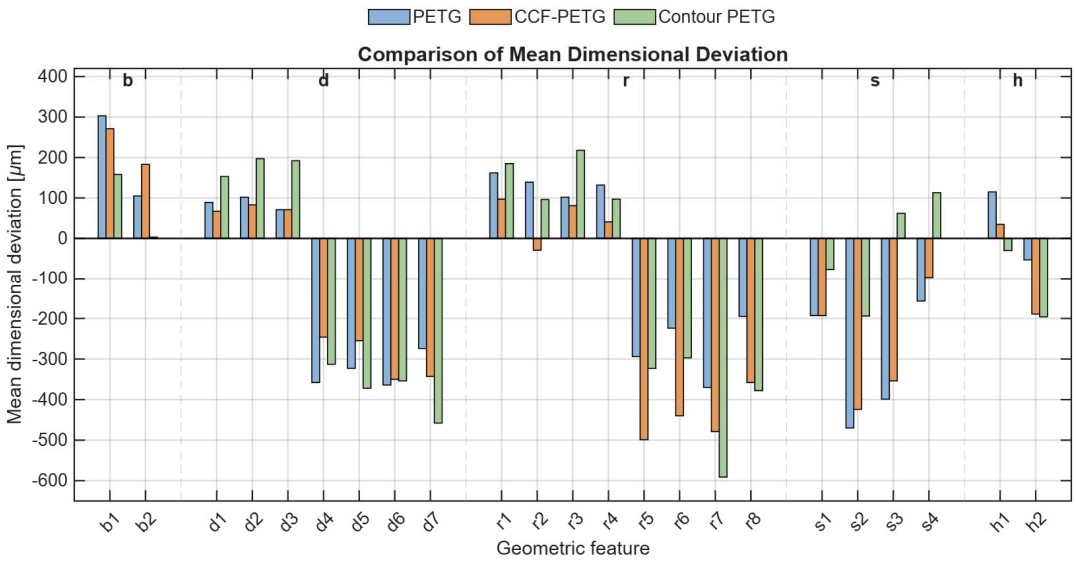

Figure 9. Mean deviation comparison per each artifact feature (dimensions are in µm)

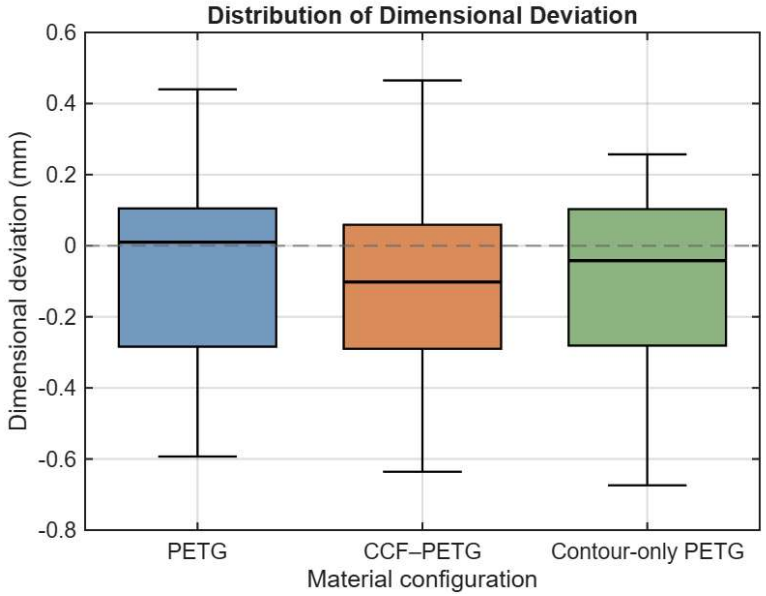

Figure 10. Distribution of dimensional deviation

For cylindrical features, Contour PETG showed the largest deviations, reaching 197 µm for boss cylinders and −458 µm for cylindrical holes, whereas PETG and CCF-PETG exhibited comparable deviations. In the case of rectangular boss features, CCF-PETG resulted in the smallest deviation, while PETG and Contour PETG showed axis-dependent variation. Rectangular hole features exhibited the largest net deviations among all feature types. For radii r5–r8, CCF-PETG showed the largest negative deviations, with r5 reaching −499 µm; r7 represented the largest net deviation across all dimensional groups. Triangular features exhibited a similar negative deviation trend to rectangular holes; however, Contour PETG showed improved accuracy compared to PETG and CCF-PETG.

For vertical (z-direction) dimension h1, PETG and CCF-PETG showed a positive deviation, 115 µm and 35 µm respectively, while the Contour PETG showed a negative deviation of −30 µm. For h2, all the material groups showed a negative deviation, the largest being Contour PETG.

The box plot in Figure 10 shows that the median deviation for PETG was slightly positive (10 µm), while CCF-PETG and Contour PETG exhibited negative median deviations of −102 µm and −42 µm, respectively. The interquartile range (IQR) was smallest for CCF-PETG (349 µm), followed by Contour PETG (384 µm), while PETG exhibited the largest IQR (389 µm). Despite these differences, the IQR values across the three materials were comparable, indicating a similar level of repeatability and accuracy.

Note: Mean deviation values were calculated using the excel spreadsheet in accordance with the following equation:

$$Mean\ Deviation\ = \frac{\sum_0^N (Actual\ value - Nomin\quad value)}{N} \quad (1)$$

5.2 Tensile testing results

Tensile testing was performed on six specimen configurations: neat PETG, 0°, 15°, 30°, and 45° continuous carbon fiber-reinforced PETG (CCF-PETG), and a contour-only CCF-PETG variant. For each group, up to three specimens were tested and the key mechanical properties were recorded (ultimate tensile strength (UTS), Young's modulus

(E), and strain at fracture). The mean values and standard deviations for all configurations are summarized in Table 3, and the following subsections discuss each property in detail.

Table 3. Summary of Mean Mechanical Properties for All Specimen Configurations

Configuration	UTS (MPa)	SD (MPa)	E (GPa)	SD (GPa)	Strain (mm/mm)
Neat PETG	44.4	4.70	3.024	0.188	0.803
0° CCF-PETG	269.3	3.44	44.62	1.160	0.199
15° CCF-PETG	228.8	22.35	37.30	6.709	0.199
30° CCF-PETG	105.0	12.79	16.32	3.037	0.199
45° CCF-PETG	92.6	4.19	14.47	0.828	0.199
Contour Only	79.4	2.47	11.11	0.521	0.199

5.2.1 Ultimate Tensile Strength

The UTS results reveal a strong and consistent dependence on fiber orientation (see Fig. 11 for the mean UTS values with error bars). The 0° CCF-PETG specimens recorded the highest mean UTS of 269.3 MPa (SD ± 3.4 MPa), representing an approximately six-fold increase over neat PETG (44.4 MPa, SD ± 4.7 MPa). This result is expected, as fibers aligned parallel to the loading direction bear the applied load most efficiently through direct tension along the fiber axis.

The 15° CCF-PETG specimens achieved a mean UTS of 228.8 MPa (SD ± 22.4 MPa), only marginally lower than the 0° group, though the considerably larger standard deviation suggests some variability between specimens due to slight fiber misalignment or inter-specimen printing inconsistencies. Beyond 15°, UTS dropped sharply: the 30° group recorded a mean of 105.0 MPa (SD ± 12.8 MPa) and the 45° group 92.6 MPa (SD ± 4.2 MPa), indicating that shear-dominated failure mechanisms become increasingly prominent as the fiber angle increases relative to the loading axis. The contour-only configuration, which lacks any infill fibers across the cross-section, exhibited the lowest mean UTS among the CCF-PETG specimens at 79.4 MPa (SD ± 2.5 MPa), though this

remained notably higher than neat PETG, demonstrating that even peripheral fiber deposition provides a meaningful strength enhancement.

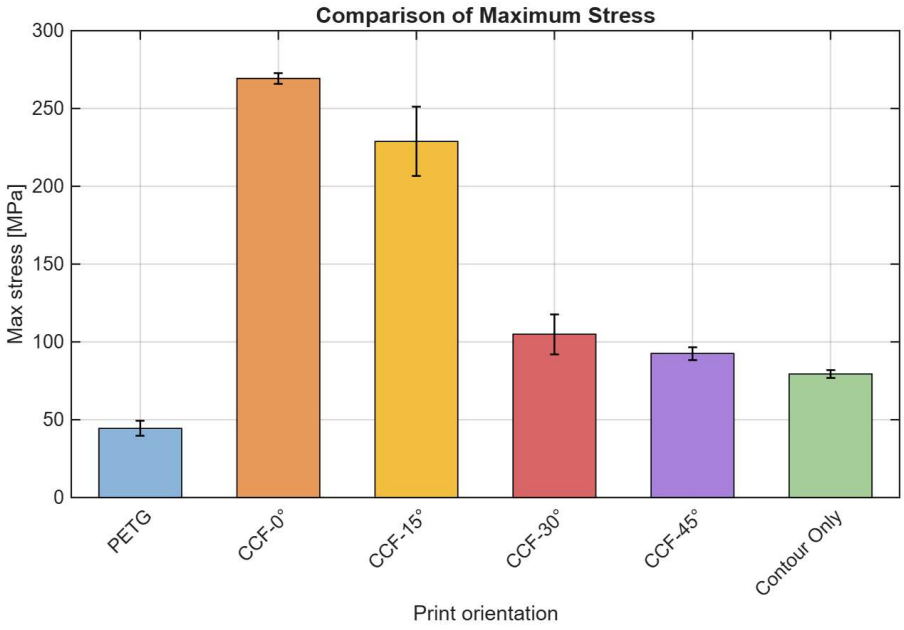

Figure 11. Mean ultimate tensile strength (MPa) by specimen configuration, with error bars representing one standard deviation. n = 3 for all groups except 0° (n = 2).

5.2.2 Young's Modulus

The stiffness results follow a trend similar to that observed for UTS (see Fig.12). The 0° CCF-PETG specimens recorded the highest mean Young's modulus of 44.6 GPa (SD ± 1.16 GPa), compared to just 30.2 GPa for neat PETG (SD ± 0.19 GPa). This dramatic improvement emphasizes the exceptionally high axial stiffness of continuous carbon fibers when oriented in the direction of loading.

Rotating the fibers to 15° reduced the mean modulus to 37.3 GPa (SD ± 6.71GPa). The large standard deviation here indicates considerable specimen-to-specimen variation, consistent with the UTS observations for this group. Further rotation to 30° and 45° yielded mean moduli of 16.32 GPa (SD ± 3.04 GPa) and 14.47 GPa (SD ± 0.83 GPa) respectively, reflecting the rapid stiffness degradation associated with off-axis loading. The contour-only specimens had a mean modulus of 11.11 GPa (SD ± 0.52 GPa), which, while lower than all fiber-infill configurations, still greatly exceeded that of neat PETG.

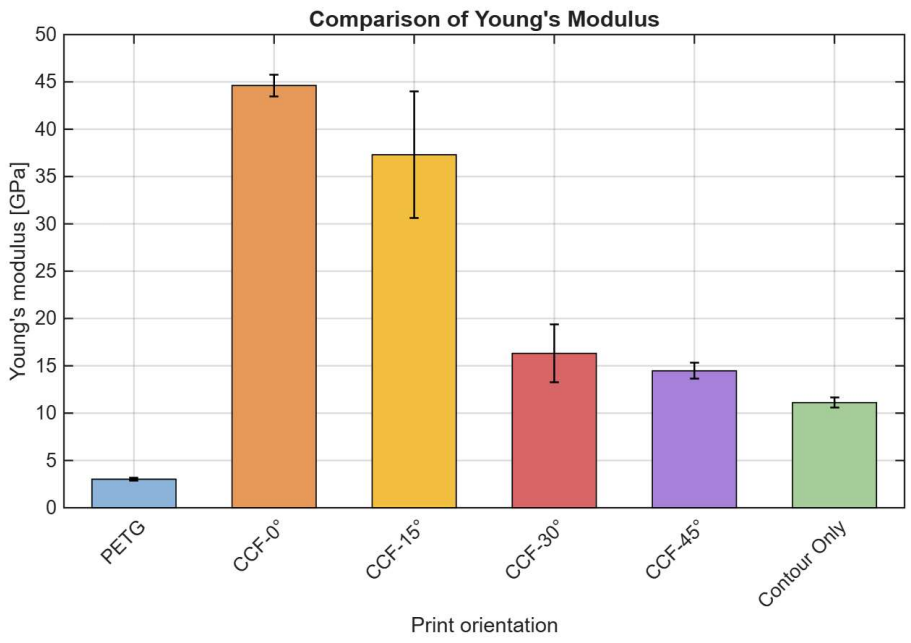

Figure 12. Mean Young's modulus (GPa) by specimen configuration, with error bars representing one standard deviation.

5.2.3 Strain at Fracture

The strain at fracture data (see Fig. 13) reveals contrast between neat PETG and the CCF-PETG configurations. Neat PETG specimens fractured at a mean strain of 0.803 mm/mm (SD ± 0.001), exhibiting considerable ductility through plastic elongation prior to failure, consistent with the behavior of an unreinforced thermoplastic.

In contrast, all CCF-PETG configurations fractured at a mean strain of approximately 0.199 mm/mm, with negligible variation between groups and specimens (SD ≈ 0 for most configurations). This four-fold reduction in failure strain relative to neat PETG is characteristic of continuous fiber-reinforced composites, where the brittle carbon fibers constrain the ductile polymer matrix and promote sudden, low-elongation fracture. The uniformity of strain across all CCF-PETG configurations suggests that fracture strain is governed primarily by the fibers themselves rather than by their orientation, in contrast to the orientation-dependent behavior observed for UTS and stiffness.

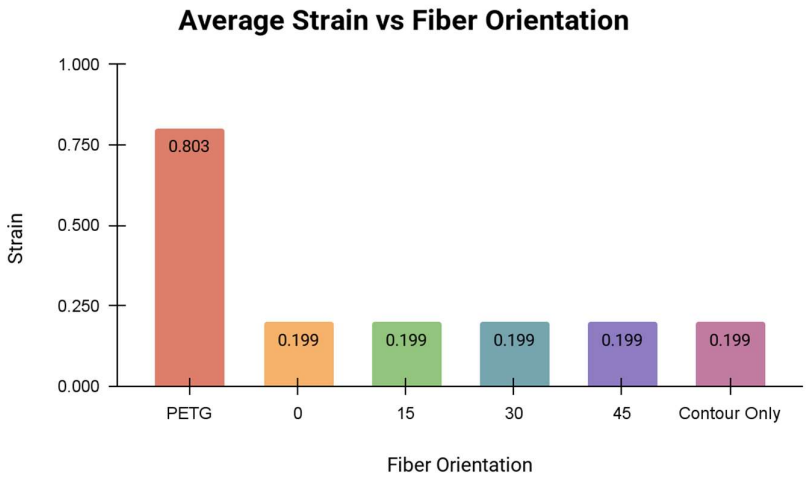

Figure 13. Mean strain at fracture (mm/mm) by specimen configuration, with error bars representing one standard deviation.

5.2.4 Inter-Specimen Variability

The 0° and 45° groups exhibited the lowest variability (SD% of 1.3% and 4.5% respectively), suggesting highly consistent specimen manufacture and failure mode for these configurations. The 15° group showed the greatest scatter (SD% ≈ 9.8%), which may be attributed to sensitivity of the off-axis failure mode to minor manufacturing inconsistencies in fiber placement during printing. It should also be noted that only two specimens were successfully tested for the 0° configuration, limiting the statistical confidence of those results; the third specimen may have experienced a premature or invalid failure during testing.

6. Analysis and Discussion

The experimental results show that a general trend in dimensional accuracy and/or deviation could not be established for the investigated materials. Although improvements were present in some dimensions and features of CCF-PETG compared to PETG, these improvements were not consistent across all axes or geometrical elements. Variations within printing speed, constraints of fiber placement, and deposition behavior linked with continuous fiber co-extrusion contributed to axis-dependent and feature-dependent deviations. Therefore, improvements noted in one direction or feature were not replicated necessarily in other directions or features. Results indicate that the effect of continuous carbon fiber reinforcement on dimensional accuracy is highly context-dependent and

governed by the interaction between material behavior, process parameters, and geometric constraints. While increased stiffness and reduced thermal deformation can provide localized improvements in dimensional stability, limitations related to minimum feature size, curvature radius, and fiber continuity can offset these benefits, particularly in complex geometries or geometries with fine features.

Note: Total deviation values were calculated using the excel spreadsheet in accordance with the following equation:

$$Total\ Deviation\ =\ Max(Deviation) - Min(Deviation\ ) \quad (2)$$

Next, the mechanical properties were thoroughly analyzed. The observed reduction in both UTS and Young's modulus with increasing fiber angle is consistent with classical laminate theory and off-axis loading mechanics. When fibers are aligned at 0° to the loading direction, the applied load is carried primarily through axial tension along the fiber, which is the highest-stiffness, highest-strength mode of loading for a carbon fiber composite. As the fiber angle increases, the load transfer shifts progressively from fiber-dominated axial tension toward matrix-dominated shear and transverse tension, both of which are governed by the weaker PETG matrix rather than the carbon fibers. This explains the steep drop in UTS from 269.3 MPa at 0° to 92.6 MPa at 45° showcasing strong angular dependence of composite strength. The uniformity of fracture strain across all CCF-PETG groups (~0.199 mm/mm, regardless of angle) further supports this interpretation: fracture is initiated by fiber failure or fiber-matrix debonding at a characteristic limiting strain, rather than by matrix yielding as in neat PETG.

Several limitations of the present study should be acknowledged. First, variability in the FFF printing process (including fiber placement accuracy, inter-layer bonding, and void content) introduces uncontrolled sources of scatter that were not quantified in this study. The notably high standard deviation in the 15° group (SD ± 22.4 MPa, equivalent to 9.8% of the mean) likely reflects such manufacturing inconsistencies. Secondly, and most significantly, one of the primary objectives of this project was to evaluate and characterize the capabilities of the Anisoprint A4 composite printer, which is a relatively novel and not yet widely adopted system. The mid-project mechanical failure of the printer therefore constituted a direct limitation on achieving this core aim, preventing a

fuller assessment of the machine's repeatability, process window, and suitability for composite part fabrication.

As a future direction, a three-point bending test programme was planned to characterize the flexural properties of the CCF-PETG configurations, and to further evaluate the Anisoprint A4 printer's capabilities across a broader range of mechanical loading conditions. This was particularly important given that one of the explicit aims of the project was to assess the Anisoprint A4 as a composite manufacturing platform, a system that, unlike more established printers, has not yet been extensively studied or benchmarked in the open literature. However, the printer became inoperative during the course of the project, preventing the fabrication of bending specimens within the capstone timeframe. As a result, the characterisation of the machine's full capabilities remains incomplete. It is intended that three-point bending tests, along with a more systematic evaluation of the Anisoprint A4's process parameters and print quality, will be pursued as a continuation of this work following the capstone project, once the printer is repaired or replaced.

7. Conclusion

In conclusion, this study indicates that continuous carbon fiber reinforcement does not necessarily ensure lower dimensional accuracy of PETG-based FFF parts. Instead, the dimensional performance must be assessed in relation to specific geometries and printing conditions. Future work will be focusing on increasing the sample number per condition, as well as a systematic optimization of process parameters using the Taguchi method of experiment, while high-precision coordinate measurement and 3D scanning systems should be used to better isolate and quantify the factors that come into consideration in governing dimensional accuracy in CCF-PETG systems.

Taken together, the tensile testing results demonstrate that both UTS and Young's modulus decrease monotonically as the carbon fiber orientation angle increases from 0° to 45° and are further reduced in the contour-only configuration. This behavior is consistent with classical laminate theory, which predicts maximum stiffness and strength when reinforcing fibers are aligned with the principal loading direction. The addition of continuous carbon fibers to PETG, even at unfavorable orientations such as 45°, consistently increases both UTS and stiffness relative to unreinforced PETG, while simultaneously reducing ductility. These results highlight the trade-off inherent in the use of CCF-PETG: substantially improved stiffness and strength at the cost of the energy-absorbing plastic deformation capacity characteristic of neat thermoplastics.

8. References

[1] **Akbas, O. Hira, S. Samankan, S. Z. Hervan, and A. Altinkaynak,** *"Dimensional accuracy of FDM-printed PLA, PETG and ABS products manufactured by different sets of printing parameters,*" European Mechanical Science, vol. 8, no. 1, pp. 11–18, 2024. doi: 10.26701/ems.1392387.

[2] **Anisoprint Aura Slicing Software** Webpage. URL: https://anisoprint.com/aura/

[3] **Anisoprint Website**. URL: https://anisoprint.com/solutions/desktop/

[4] **Bex, G. J., Ingenhut, B. L., Ten Cate, T., Sezen, M., & Ozkoc, G. (2021).** *Sustainable approach to produce 3D-printed continuous carbon fiber composites:"A comparison of virgin and recycled PETG".* Polymer Composites, 42(9), 4253-4264.

[5] **CMT-50 Universal Testing Machine documentation**. URL: https://pdf.directindustry.com/pdf/jinan-liangong-testing-technology-co-ltd/universal-testing-machine-cmt-10-cmt-50/180963-967525.html

[6] **Cuan-Urquizo, E., Barocio, E., Tejada-Ortigoza, V., Pipes, R. B., Rodriguez, C. A., & Roman-Flores, A. (2019)**. C*haracterization of the mechanical properties of FFF structures and materials: A review on the experimental, computational and theoretical approaches.* Materials, 12(6), 895.

[7] **Cuan-Urquizo, C. Barocio, R. Tejada-Ortigoza, J. R. Curiel-Sosa, L. L. Lopes, and W. R. Zhong,** *"Characterization of the Mechanical Properties of FFF Structures," Materials,* vol. 12, no. 6, 2019. doi: 10.3390/ma12060953.

[8] **Dairabayeva, D.;Auyeskhan, U.; Talamona, D.** *Mechanical Properties and Economic Analysis of Fused Filament Fabrication Continuous Carbon Fiber Reinforced Composites. Polymers 2024*, 16, 2656. https://doi.org/10.3390/polym16182656

[9] **Dimitrios, C. H. A. I. D. A. S., Mastorakis, N. I. K. O. S., & Kechagias, J. O. H. N. (2016).** *The impact of temperature changing on dimensional accuracy of FFF process. International Journal of Applied Physics, 1, 1-5.*

[10] **Fallah, Q. Saleem, and B. Koc,** *"Mechanistic modeling and nonlinear mechanical behavior of continuous carbon fiber reinforced PETG,"* Composites Part B, vol. 243, 110468, 2022. doi: 10.1016/j.compositesb.2022.110468.

[11] **Iacob, D. V., Zisopol, D. G., & Minescu, M. (2025).** *Study on the Optimization of FDM Parameters for the Manufacture of Three-Point Bending Specimens from PETG and Recycled PETG in the Context of the Transition to the Circular Economy. Polymers, 17(12), 1645*. https://doi.org/10.3390/polym17121645

[12] **Jamal, P. Rajesh, and S. K. Singh,** *"Additive Manufacturing of Fiber-Reinforced Composites: A Comprehensive Review,"* Polymers for Advanced Technologies, 2024. doi: 10.1002/pat.6441.

[13] **Jamal, M.A.; Shah, O.R.; Ghafoor, U.; Qureshi, Y.; Bhutta, M.R.** *Additive Manufacturing of Continuous Fiber-Reinforced Polymer Composites via Fused Deposition Modelling: A Comprehensive Review.* Polymers 2024, 16, 1622. https://doi.org/ 10.3390/polym16121622

[14] **Kasmi, G. Ginoux, S. Allaoui, and S. Alix,** *"Investigation of 3D printing strategy on the mechanical performance of coextruded continuous carbon fiber composite filament,"* Journal of Applied Polymer Science, vol. 138, no. 38, 50955, 2021. doi: 10.1002/app.50955.

[15] **Lupone, F.; Padovano, E.; Venezia, C.; Badini, C.** *Experimental Characterization and Modeling of 3D Printed Continuous Carbon Fibers Composites with Different Fiber Orientation Produced by FFF Process.* Polymers 2022, 14, 426. https://doi.org/10.3390/polym14030426

[16] **Mahesh, A. S. Joseph, V. Mahesh, D. Harursampath, and C. V. N. Rao,** *"Experimental evaluation of flexural properties of 3D printed parts via fused filament fabrication,"* Materials Today: Proceedings, 2023. doi: 10.1016/j.matpr.2023.02.262.

[17] **Mangalampalli, S. Gupta, A. Indalkar, A. J. Arputham, and B. Kandasubramanian,** *"Advances in Additive Manufacturing of Carbon Fiber-Reinforced PETG Composites: Mechanical Properties and Industrial Applications," Polymers for Advanced Technologies,* 2025. doi: 10.1002/pat.70201.

[18] **O'Driscoll, C., Owodunni, O., & Asghar, U. (2024).** *Optimization of 3D printer settings for recycled PET filament using analysis of variance (ANOVA).* Heliyon, 10(5).

[19] **Paneva, M., Panev, P., & Tsonev, V. (2025).** *Tensile Testing of Polymer Material Specimens Obtained by Fused Deposition Modeling. Engineering Proceedings,* 100(1), 50. https://doi.org/10.3390/engproc2025100050

[20] **Polymaker PolyLite™ PETG Filament Manufacturer website.** URL: https://wiki.polymaker.com/polymaker-products/polymaker-filaments/prime-materials/petg/polylite-tm-petg

[21] **Raj, S. Anand, and M. N. Gokhale**, *"Mechanical properties and dimensional deviations in FDM of PETG with machine-learning prediction models," Coatings*, vol. 15, no. 1117, 2025. doi: 10.3390/coatings15091117.

[22] **Rijckaert, S.; Daelemans, L.; Cardon, L.; Boone, M.; Van Paepegem,W.; De Clerck, K.** *Continuous Fiber-Reinforced Aramid/PETG 3D-Printed Composites with High Fiber Loading through Fused Filament Fabrication.* Polymers 2022, 14, 298. https://doi.org/10.3390/polym14020298

[23] **"Software used for StaabTEC." StaabTEC**. https://www.staabtec.de/en/3d-software.html (accessed Nov. 30, 2025).

[24] **SolidWorks 2025 CAD software webpage.** URL: https://www.solidworks.com/product/whats-new-2025

[25] **Valvez, A. Silva, and P. Reis,** *"Effect of layer thickness and printing parameters on mechanical properties of PETG parts fabricated via FFF," Polymers*, vol. 13, no. 1213, 2021. doi: 10.3390/polym13081213.

[26] **Yankin, A., Alipov, Y., Temirgali, A., Serik, G., Danenova, S., Talamona, D., & Perv een, A. (2023).** *Optimization of printing parameters to enhance tensile properties of ABS and nylon produced by fused filament fabrication. Polymers*, *15*(14), 3043.

[27] **Zeiss T-SCAN Technical Data**. URL: https://www.handsonmetrology.com/products/t-scan/#Technical_Data

[28] **Razali, N.M., Wah, Y.B.** Power comparisons of Shapiro–Wilk,Kolmogorov–Smirnov, Lilliefors and Anderson–Darling tests. Journal of Statistical Modeling and Analytics 2(1) (2011) 21–33.

9. Appendix A. Mean dimensional deviation data.

Table 4. Surface comparison results

Feature (nominal dimension, mm)	PETG mean (µm)	PETG SD (µm)	CCF-PETG mean (µm)	CCF-PETG SD (µm)	Contour-only PETG mean (µm)	Contour-only PETG SD (µm)
b1 (85.00)	303	139	271	112	158	55
b2 (85.00)	105	74	183	176	3	26
d1 (22.50)	89	41	67	41	153	58
d2 (22.50)	102	38	83	34	197	66
d3 (22.50)	71	31	71	25	192	45
d4 (14.50)	-358	33	-246	59	-313	59
d5 (14.50)	-323	34	-255	57	-372	46
d6 (22.50)	-364	32	-350	206	-354	47
d7 (17.00)	-274	43	-343	113	-458	56
r1 (22.50)	162	72	97	45	185	61
r2 (10.00)	139	92	-29	78	96	81
r3 (22.50)	102	84	81	31	218	27
r4 (10.00)	132	89	41	25	97	63
r5 (22.50)	-294	96	-499	57	-323	36
r6 (10.00)	-224	105	-440	82	-297	44
r7 (16.50)	-370	138	-479	89	-591	67
r8 (4.00)	-195	93	-358	106	-378	50

s1 (25.00)	-193	52	-193	135	-77	32
s2 (25.00)	-470	79	-424	130	-194	37
s3 (25.00)	-399	70	-354	96	62	88
s4 (25.00)	-157	126	-97	132	113	63
h1 (4.04)	115	55	35	77	-30	33
h2 (8.20)	-53	42	-189	57	-196	35

10. Appendix B. Surface comparison data.

Table 5. Surface comparison results

PETG Artifacts	CCF PETG Artifacts